Cellulose (2009) 16:227–238
DOI 10.1007/s10570-008-9269-6

A new bio-based nanocomposite: fibrillated TEMPO-oxidized celluloses in hydroxypropylcellulose matrix

Richard K. Johnson · Audrey Zink-Sharp · Scott H. Renneckar · Wolfgang G. Glasser

Received: 13 May 2008 / Accepted: 23 November 2008 / Published online: 17 December 2008

Abstract Utilization of TEMPO-oxidized celluloses in bio-based nanocomposites is reported for the first time. TEMPO-oxidized wood pulps (net carboxylate content 1.1 mmol/g cellulose) were fibrillated to varying degrees using a high intensity ultrasonic processor. The degree of fibrillation was controlled by varying sonication time from 1 to 20 min. The sonication products were then characterized independently and as fillers (5 wt% loading) in hydroxypropyl cellulose nanocomposite films. Nanofibril yields ranging from 11 to 98 wt% (on fiber weight basis) were obtained over the range of sonication times used. Suspension viscosities increased initially with sonication time, peaked with gel-like behavior at 10 min of sonication and then decreased with further sonication. The thermal degradation temperature of unfibrillated oxidized pulps was only minimally affected (6 °C decrease) by the fibrillation process. Dynamic mechanical analysis of the nanocomposites revealed strong fibril-matrix interactions as evidenced by remarkable storage modulus retention at high temperatures and a suppression of matrix glass transition at "high" (~5 wt%) nanofibril loadings. Creep properties likewise exhibited significant (order of magnitude) suppression of matrix flow at high temperatures. It was also believed, based on morphologies of freeze-fracture surfaces that the nanocomposites may be characterized by high fracture toughness. Direct fracture testing will however be necessary to verify this suspicion.

Keywords TEMPO · Sonication · Nanocomposites · Nanofibrils · Fibrillated · Cellulose

R. K. Johnson
Macromolecular Science and Engineering, Virginia Polytechnic Institute and State University, 230 Cheatham Hall, Blacksburg, VA 24061-0323, USA

A. Zink-Sharp (✉) · S. H. Renneckar · W. G. Glasser
Department of Wood Science and Forest Products, Virginia Polytechnic Institute and State University, 230 Cheatham Hall, Blacksburg, VA 24061-0323, USA
e-mail: agzink@vt.edu

Introduction

When composite materials are fully derived from bio-based components, desirable benefits such as biodegradability and biocompatibility are emphasized. Proceeding from such interests is the development of nanocomposites derived from nanoscale cellulosic elements in bio-based polymer matrices (Matsumura et al. 2000; Gindl and Keckes 2005; Petersson and Oksman 2006; Wibowo et al. 2006). So far, the most commonly used nanocelluloses are microfibrillated celluloses (MFCs) (Zimmermann et al. 2004; Svagan et al. 2007) and cellulose nanocrystals (CNCs) (Grunert and Winter 2002; Petersson and Oksman 2006; Petersson et al. 2007). MFCs are produced by a two-step process: mechanical refining of wood and

natural fiber pulps followed by several passes through a high intensity homogenizer (Herrick et al. 1983; Turbak et al. 1983; Nakagaito and Yano 2005). The product is a dense network of highly fibrillated celluloses ranging from 10 to 100 nm in width. CNCs on the other hand, are generated from acid hydrolysis of pulp fibers. The hydrolysis process dissolves amorphous regions in the fiber leaving intact the crystalline fraction (Edgar and Gray 2003). The nanocrystalline suspensions are washed and further homogenized by ultrasonic treatment.

Recently, Saito et al. (2006) reported their discovery of individualized cellulose nanofibrils following homogenization of oxidized cellulose fibers. Cellulose fibers were oxidized via the 2,2,6,6-tetramethylpiperidine-1-oxyl (TEMPO)-mediated oxidation process, which converts primary alcohols to aldehydes and carboxylate groups. When polysaccharides such as cellulose are oxidized in an aqueous medium, a primary oxidant, commonly sodium hypochlorite (NaOCl) is needed for in situ activation of the TEMPO radical (Bragd et al. 2004). NaOCl concentrations in the range of 2.5–3.8 mmol/g cellulose allowed for nanofibrillation of more than 90% of wood and cotton fibers (Saito et al. 2006). The nanofibrils from wood pulp ranged from 3 to 5 nm in width and several hundred nanometers to a few microns in length. Ease of fibril disintegration was attributed to interfibrillar repulsive forces generated by surface carboxylate groups. With the exceptionally small fibril widths, the homogenized oxidized cellulose suspensions appeared transparent. It has also been reported that TEMPO-mediated oxidation produces no change in crystallinity of cellulose even at a high oxidation level of 10 mmol NaOCl/g cellulose (Saito and Isogai 2004). Unlike conventional microfibrillation and acid hydrolysis processes which yield microfibril networks and short crystallite bundles, respectively, fibrillated celluloses from TEMPO-mediated oxidation generate long individualized nanofibrils with diverse surface functionalities (carboxyl, aldehyde, and hydroxyl). We perceive that the unique physical and chemical characteristics of these fibrillated oxidized celluloses could offer significant potential in the fields of coatings, composites reinforcement, packaging, and drug delivery.

Utilization of TEMPO-oxidized celluloses as nanofillers in a bio-based polymer matrix was the subject of this study. Properties of fiber-reinforced composites depend on a variety of factors which include fiber dimensions, fiber volume fraction, and fiber-matrix interfacial adhesion. Since TEMPO-mediated oxidation of pulp produces easily fibrillated products, regulating exposure time to a homogenizer can be used to control the nanofibril fraction within a fixed volume of oxidized pulp. This approach to controlling nanofibril volume fraction can be used for controlling properties of nanocellulose-filled biopolymer composites. Nakagaito and Yano (2005) have previously investigated the influence of fibrillation degree on cellulose nanocomposite properties using phenol formaldehyde-bonded MFC mats. They controlled the degree of MFC fibrillation by varying the number of passes through (1) a refiner only and (2) a refiner followed by a homogenizer. A significant increase in bending strength was found when MFCs underwent 30 passes through the refiner and subsequent passes through the homogenizer. Young's modulus on the other hand was only marginally influenced. Morphological studies on the MFCs revealed that fibrillation of the starting pulp fibers was only superficial when the number of refiner passes was fewer than 16. By 30 passes, the bulk of the pulp fibers had fibrillated into fine nanofibril networks, which provided the needed surface area for the observed strength enhancement. In the present paper, ultrasonication was employed to fibrillate TEMPO-oxidized cellulose fibers of a softwood pulp. Nanofibril volume fraction was controlled by varying sonication time. The fibrillated products were utilized as reinforcing fillers in solvent-cast hydroxypropyl cellulose (HPC) films, which were then evaluated by dynamic mechanical and creep compliance testing.

Experimental

Materials

Never-dried kraft pulp (Douglas-fir) served as starting cellulose fiber. The pulp of 85% brightness was kindly provided by Weyerhaeuser Company, Washington, USA. Further bleaching of the pulp was achieved in acidified sodium chlorite solution using the method of Wise et al. (1946). The samples were preserved in a refrigerator below 8 °C until used. Sulfite pulp (Tembec Inc Temalfa 95A) was used for preparation of CNCs.

HPC (average M_w = 100,000 g/mol, molar substitution 3.4–4.4 propylene oxide groups per anhydroglucose unit), TEMPO, NaOCl, NaBr, HCl, NaOH, and ethanol were purchased from Sigma–Aldrich and used as received.

Methods

TEMPO-mediated oxidation

Never-dried pulp (20 g fiber weight, 123 mmol primary alcohol) was suspended in 800 mL of high purity water (resistivity at 25 °C = 18.2 MΩ cm) and agitated with an overhead stirrer operating at 500 rpm. A 10 mL aqueous solution of TEMPO (0.25 g, 1.60 mmol) and NaBr (2.5 g, 24.3 mmol) was prepared, added to the pulp suspension, and the mixture was stirred continuously for about 5 min. A 12.4% NaOCl solution (39.8 mL, 4.00 mmol available Cl per gram cellulose) was added drop-wise to the mixture while maintaining a pH of 10 ± 0.2 with addition of 0.5 M NaOH solution. After about 50 min, no further change in pH was observed, indicating the end of the reaction. Ethanol (30 ml) was then added to fully quench the reaction and the pH was adjusted to 7.0 with a 0.5 M HCl solution. The suspension was vacuum-filtered, washed several times with deionized water and stored at <8 °C until used. Appearance and morphology of oxidized product were similar to those of the starting pulp fibers.

Fibrillation of oxidized fibers

Oxidized fibers were first milled to 60 mesh (250 μm) sizes using a Wiley® mini-mill. Fiber suspensions (0.3 wt% solids) were prepared by dispersing 0.5 g milled fibers in 150 mL of deionized water. The suspensions were sonicated with a Sonics® ultrasonic processor (Model GE 505) for varying amounts of time (details in Table 1). A double-walled glass beaker connected to a circulating ice water bath was used to prevent overheating of suspension during sonication (schematic of setup shown in Fig. 1). Sonicated suspensions were stored at <8 °C in plastic bottles until used.

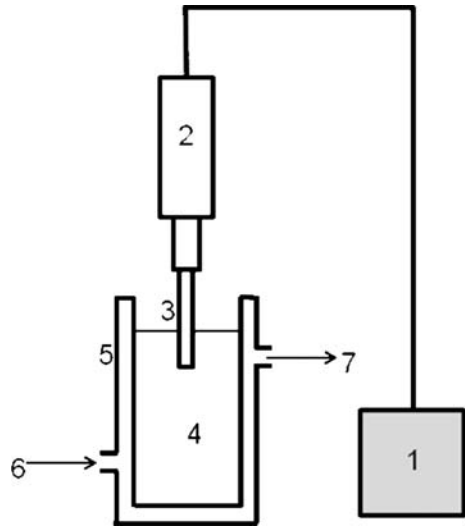

Fig. 1 Schematic of ultrasonication setup for cellulose fibrillation. (*1*) power control, (*2*) piezoelectric converter, (*3*) ultrasonic probe, (*4*) cellulose suspension, (*5*) double-walled glass beaker, (*6*) ice water inlet and (*7*) outlet

Preparation of CNCs and MFCs

CNC preparation followed a previously reported method (Beck-Candanedo et al. 2005). MFCs were

Table 1 Yields from sonication and weight fractions in nanocomposites of nanofibrils and UPFs. Standard deviations for three replications are shown in parentheses

Sonication time (min)	Nanofibrils		UPFs	
	Yield (%)[a]	Weight fraction (%)[b]	Yield (%)	Weight fraction (%)
1	10.5 (1.2)	0.52	88.8 (0.7)	4.44
5	41.7 (3.2)	2.08	57.1 (3.3)	2.85
10	86.5 (2.0)	4.33	12.9 (2.6)	0.64
15	96.8 (0.7)	4.84	3.0 (0.7)	0.15
20	97.5 (1.0)	4.88	2.5 (1.4)	0.12

[a] Calculated according to Eq. 1

[b] Weight fractions in nanocomposites carrying total fiber content of 5 wt%

prepared from the original pulp stock used for TEMPO-mediated oxidation. Pulp suspensions (0.25 wt%) were dispersed in deionized water and fibrillated by 20 passes through a high intensity homogenizer (Microfluidics M-110 EH) operated at 30,000 psi i.e. ~207 MPa.

Characterization of fibrillated fibers

Yield Sonicated suspensions were centrifuged at 4,550*g* rcf for 20 min to separate the nanofibrils (in supernatant fraction) from unfibrillated and partially fibrillated fibers (referred to as UPFs henceforth) in the sediment fraction. The separated fractions were dried to constant weight at 50 °C in a forced air oven and yields (i.e. solids content after drying) were calculated according to Eq. 1.

$$\text{Yield, } \% = \frac{\text{weight of dried solids}}{\text{initial fiber weight}} \times 100 \quad (1)$$

Yield results represent averages of three replications.

Transparency Light transmittance through sonicated suspensions was measured in a UV–VIS spectrophotometer (Thermo Scientific Corporation Evolution 300). The instrument was operated in transmission mode using a Xenon light source. Data were collected in the visible region (400–800 nm).

Morphology Nanofibrils and UPFs were imaged by transmission electron microscopy (TEM) and scanning electron microscopy (SEM), respectively. Ten microliter drops of supernatant suspensions (0.01 wt%) were placed on formvar-coated copper grids (300 mesh). Prior to complete drying, the specimens were stained with uranyl acetate negative stain (2%). The samples were imaged in a Philips EM 420 transmission electron microscope operating at 100 kV. Images were acquired electronically with an installed CCD camera. SEM samples were prepared by dropping 50 μL sediment suspensions (0.01 wt%) onto clean silicon wafers followed by air-drying for 24 h. Samples were pre-coated with 3 nm gold-palladium sputter prior to imaging in a LEO Zeiss1550 field emission scanning electron microscope.

Thermal stability A thermogravimetric analyzer (TA Instruments Q 500) was used to monitor the thermal degradation behavior of the sonicated celluloses. Freeze-dried samples 10–12 mg from each treatment level were used. Thermogravimetric analysis (TGA) tests were performed in air at a heating rate of 20 °C/min. Accuracy of thermal degradation temperature was enhanced by selecting the high resolution-dynamic mode which automatically adjusts the heating rate when the instrument senses a weight loss.

Flow Flow properties of sonicated suspensions were measured with a Brookfield Viscometer (model DV-II + Pro). The small sample adapter accessory was used to achieve rapid and precise temperature control and to improve accuracy of viscosity measurements. The experiments were conducted on 10 mL samples at shear rates of 6.8–68/s. An external temperature control unit was used to maintain the experimental temperature of 25 ± 0.1 °C.

Composite film preparation

An HPC solution (7 wt%) was prepared by dissolving 70 g HPC in ~1 L deionized water. The solution was stirred overnight to ensure complete dissolution of the polymer. Fibrillated fiber suspensions were mixed with appropriate amounts of HPC solution to yield 5 wt% fiber loadings. The blends were transferred into polystyrene petri dishes (150 cm diameter) and dried at 35 °C in a forced air oven. Dried films (~0.5 mm thick), were recovered after 6–7 days and further conditioned at 50% relative humidity for 24 h.

Film characterization

Viscoelastic properties Dynamic mechanical and creep properties were measured in tension using a TA Instruments 2980 Dynamic Mechanical Analyzer. Specimen widths and lengths of 5.0 ± 0.1 and 18 ± 0.5 mm, respectively were used. Dynamic measurements were made from 0 to 150 °C at a 5 °C/min heating rate and 1 Hz. Ten minute-creep data were collected at multiple temperatures under a 0.60 MPa stress.

Morphological properties Some of the creep and dynamic mechanical specimens were embrittled in liquid nitrogen and fractured in cross-section for

SEM observations. Samples were adhered onto silicon wafers and sputter coated as previously described.

Results and discussion

Fibrillated celluloses from TEMPO-oxidized wood pulp were mechanically derived using ultrasonication. By means of conductometric titration (Katz et al. 1984), the carboxylate concentration of the oxidized pulp was calculated as 1.1 mmol/g cellulose. This is well within the oxidation range (0.99–1.23 mmol/g) earlier reported for effective disintegration (Saito et al. 2006). Nanofibril fraction in the pulp suspensions were controlled by varying sonication time. Biopolymer-based nanocomposites films using HPC as a matrix and the fibrillated oxidized celluloses as fillers were fabricated. Characteristics of the ultrasonication products as well as dynamic mechanical and creep properties of the nanocomposite films are presented. Oxidized cellulose nanocomposites are also compared with those containing CNCs and MFCs as fillers.

Fibrillated oxidized cellulose properties

Nanofibril yields of 10.5–97.5 wt% were obtained compared with 88.8–2.5 wt% UPFs from the sonication process (Table 1). Yield calculations from Eq. 1 reveal a linear dependence of yield on sonication time in the range of 1–10 min sonication (Fig. 2).

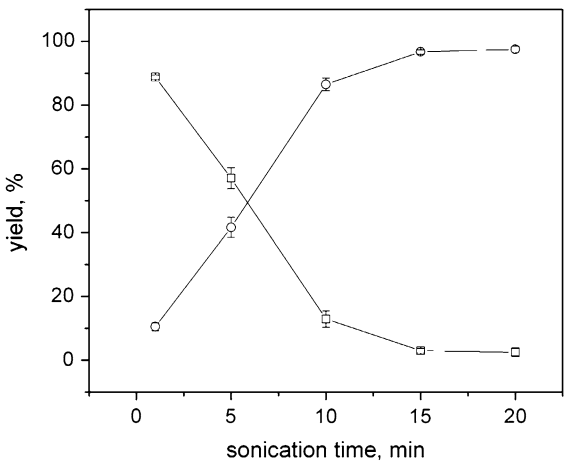

Fig. 2 Yields of nanofibrils (*circles*) in supernatant fractions and of UPFs (*squares*) in sediment fractions. Yields were calculated from Eq. 1 using weight of starting material as basis

Increasing the sonication time beyond 10 min results in a nearly 100% conversion to nanofibrils, as evidenced by the 96.7 and 97.5 wt% yields at 15 and 20 min sonication times, respectively. It appears ten minutes of sonication is sufficient to convert the bulk of the oxidized pulp fibers into nanofibrils. It is important to note that changing probe size and volume of material to be processed may result in different yield responses to sonication time.

Appearances of sonicated suspensions after standing for 24 h are depicted in Fig. 3a. Corresponding light transmittance data collected in the visible range of a UV–VIS spectrophotometer are also displayed in Fig. 3b. A substantial increase (*ca*. 65%) in transparency is observed when sonication time is increased

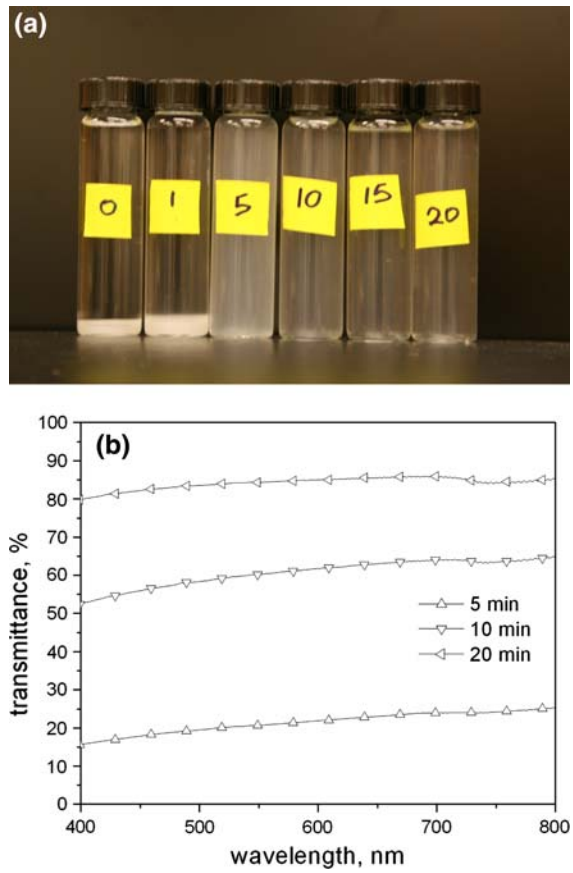

Fig. 3 **a** Fibrillated cellulose suspensions (0.3 wt% solids) 24 h after sonication. *Labels* represent sonication times in minutes. **b** Transmittance spectra for 5, 10, and 20 min sonicated suspensions in (**a**) recorded in the visible region with a UV–VIS spectrophotometer

from 5 to 10 min. This is equivalent to a >50% increase in nanofibril content (Table 1). In the previous report of (Saito et al. 2006), transparencies of TEMPO-oxidized suspensions were also found to increase with increasing degree of oxidation.

Electron micrographs of nanofibrils and UPFs were acquired with TEM and SEM, respectively. Individualized nanofibrils with shapes and sizes similar to those from previous reports (Saito et al. 2006, 2007) are observed (Fig. 4a). Using an image processing software, nanofibril widths of between 2.5 and 4 nm were measured. However, no solitary nanofibrils suitable for length measurements could be identified. The UPFs on the other hand vary widely in morphology as would be expected of fibers undergoing fibrillation under intense

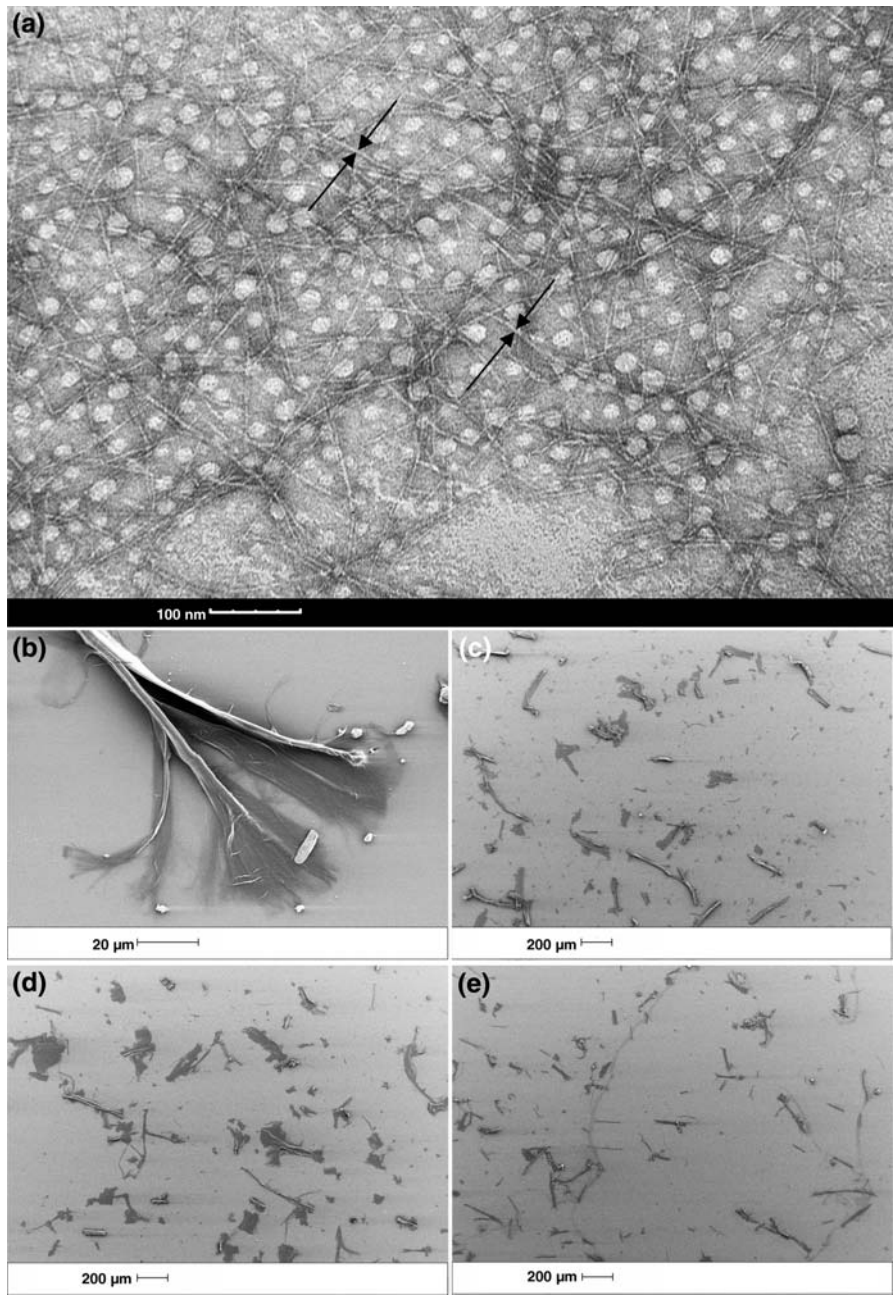

Fig. 4 Electron micrographs of fibrillated celluloses. **a** TEM of supernatant fractions showing nanofibrils of widths 2.5–4 nm (indicated with *arrows*); SEM of **b** single fiber from sediment fraction undergoing disintegration and **c–e** 0.01 wt% sediment fractions for 1, 10, and 20 min sonication times, respectively

mechanical stresses. Partially fibrillated fibers having an appearance similar to the example shown in Fig. 4b were encountered frequently in the sediment fractions. Similar broom-like structures were also observed from light microscopy images (not shown). This pattern of disintegration suggests that a simultaneous fibrillation-axial splitting of the fiber walls precedes a complete conversion of the fiber wall into nanofibrils. Images c, d, and e of Fig. 4 depict sediment fractions of 1, 10, and 20 min sonication times, respectively. Both unfibrillated and partially fibrillated fibers were seen at every level of sonication. However, the proportion of unfibrillated fibers decreased drastically when sonication times reached 15 and 20 min. A crude estimation of unfibrillated fiber dimensions from SEM imaging was made using the SEM image acquisition software. Average lengths and widths of 262 ± 156 and 24.2 ± 7 μm, respectively were determined for the ~80 fibers measured. These length averages are representative of the 60 mesh sizes of the starting fibers.

TEMPO-oxidized celluloses undergo multiple degradation events as revealed by linear (Fig. 5a) and differential (Fig. 5b) weight loss versus temperature TGA plots. Reports describing similar degradation patterns have been made for oxidized celluloses prepared from other methods (Varma and Chavan 1995; El-Sakhawy 2000; Kumar and Yang 2002) and for sulfuric acid-hydrolyzed CNCs (Wang et al. 2007). El-Sakhawy (2000) attributed these multiple degradation events to early dehydration, fragmentation, and ultimately to decomposition of carbohydrate residues. The main degradation temperatures of TEMPO-oxidized celluloses occur in the range of 225–231 °C (Fig. 5b) and represent a drastic decline from the degradation temperature (318 °C) of the unoxidized wood pulp (plot not shown). The narrow difference (6 °C) in peak degradation temperatures implies a rather weak dependence of thermal degradation temperature on nanofibril weight fraction. On the other hand, the degradation rate (weight loss per unit rise in temperature, shown as peak heights in Fig. 5b) increases with increasing sonication time or nanofibril fraction. This can be attributed to the high surface area accompanying the nanofibrillation process, which increases the effective mass of cellulose consumed per unit rise in temperature.

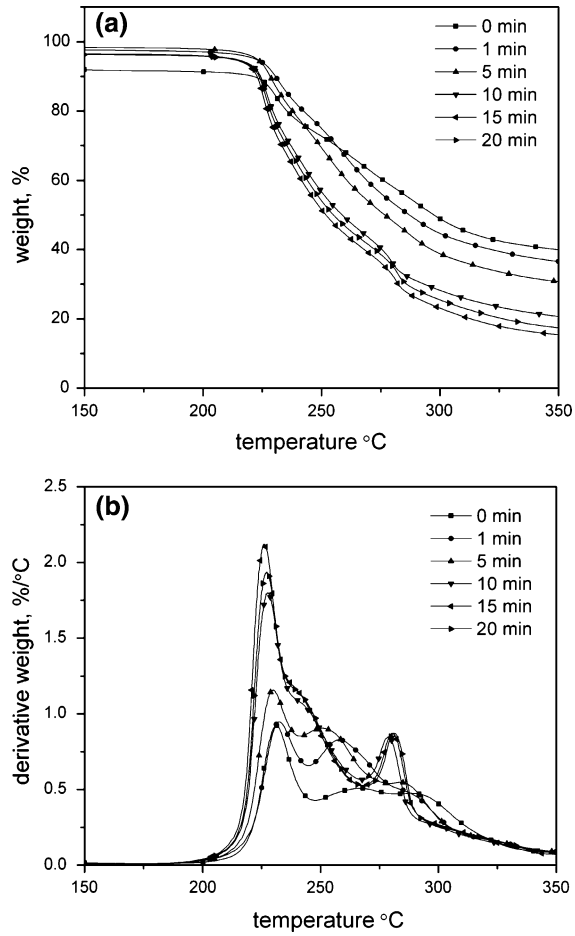

Fig. 5 Thermal degradation behavior of freeze-dried TEMPO-oxidized pulp **a** weight loss and **b** derivative of weight loss as a function of temperature. Ramp rate = 20 °C/min. *Legend* shows sonication times of starting pulp suspensions

Viscosity measurements revealed that suspension viscosities increased (to a maximum) with increasing sonication time and then started to decline with further sonication (Fig. 6). At the maximum viscosity (10 min sonication), the sonicated suspensions exhibited a gel-like character that could be readily distinguished (visually) from suspensions treated at other sonication times. The initial rise to a maximum viscosity can be attributed to the increasing proportion of high surface area nanofibrils that strongly interact with the aqueous medium. Additional energy input from longer sonication times disperses the nanofibrils which may have existed in the suspension as networks (having gel-like behavior) at the peak viscosity. In the earlier report of (Saito et al. 2007),

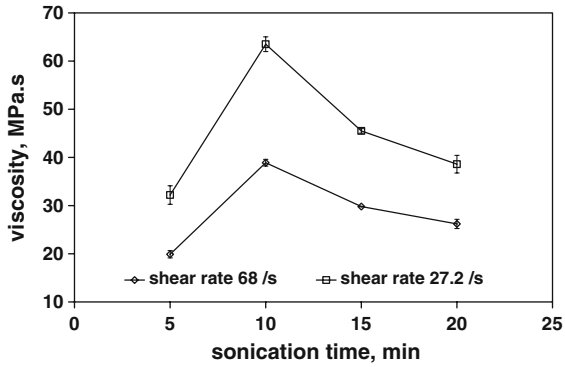

Fig. 6 High and low shear rate viscosity dependencies on sonication time of nanofibril suspensions. No data could be obtained for the 1 min sonicated suspension because its viscosity was insufficient for the minimum operating torque of the viscometer

0.1 w/v% TEMPO-oxidized pulp suspensions were magnetically stirred over periods ranging from a few hours to several days. Viscosity rose sharply from 0 to 12 h, achieved a maximum in 3 days, and declined steadily with continuous stirring to 10 days. It was recently reported that the high viscosities of TEMPO-oxidized nanocellulose suspensions could be restored by storing the suspensions at a low temperature (5 °C) for an extended amount of time (5 weeks) (Lasseuguette et al. 2008).

Composite films properties

The tensile storage moduli (E′) of nanocomposites increase with sonication time up to a limit (Fig. 7). No increases in E′ are observed at sonication times greater than 10 min (notice overlap of the 10 and 20 min E′ curves in Fig. 7). These results indicate that a sonication time of 10 min, at which close to 90 wt% of the starting fibers have been converted to nanofibrils, is sufficient for maximum E′ performance. Over the experimental temperature range (0–150 °C), the relationship between E′ and sonication time is found to be linear in the limits of 1–10 min sonication (Fig. 8). This also implies a linear dependence of E′ on nanofibril weight fraction according to the yield-sonication time relationship of Fig. 2. The data in Fig. 8 reveal more effective nanofibril reinforcements at higher temperatures (100 and 150 °C) as shown by the stronger dependence of E′ (steeper slopes of regression lines) on sonication time. This is a commonly observed effect in cellulose-based

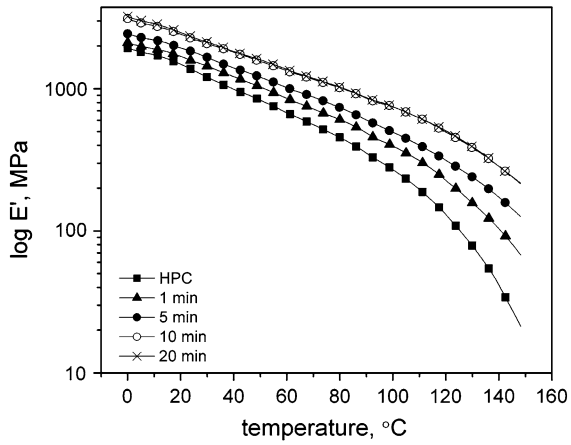

Fig. 7 Storage modulus response to temperature of HPC and nanocomposites. *Legend* shows sonication times of starting pulp suspensions. See Table 1 for corresponding nanofibril and UPF contents

nanocomposite systems found in several cellulose-based nanocomposite reports (Favier et al. 1995; Helbert et al. 1996; Chazeau et al. 1999; Samir et al. 2004; Ljungberg et al. 2005; Dalmas et al. 2007; Svagan et al. 2007).

High temperature (150 °C) E′ comparisons between oxidized cellulose nanocomposites and their CNCs and MFCs counterparts were also made. As shown by the data in Table 1, the nanofibril fraction at all levels of sonication fall short of the maximum 5 wt% in the CNC and MFC-based films. In the latter materials, all of the reinforcing elements are constituted of nanosized fillers whereas in the sonicated suspensions, only a fraction of the reinforcing fillers

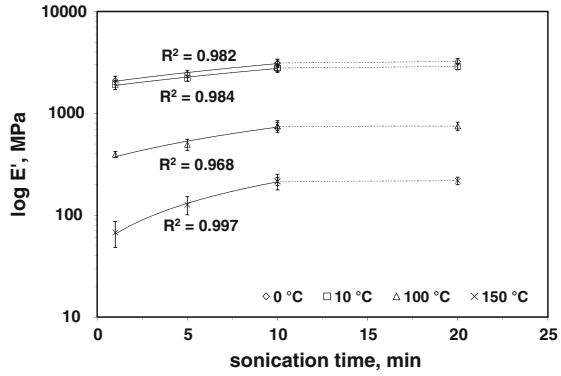

Fig. 8 Dependence of storage moduli on sonication times at low (0 and 10 °C) and high (100 and 150 °C) temperature regimes. *Solid regression lines* show regions of linear dependencies and their corresponding R^2 values

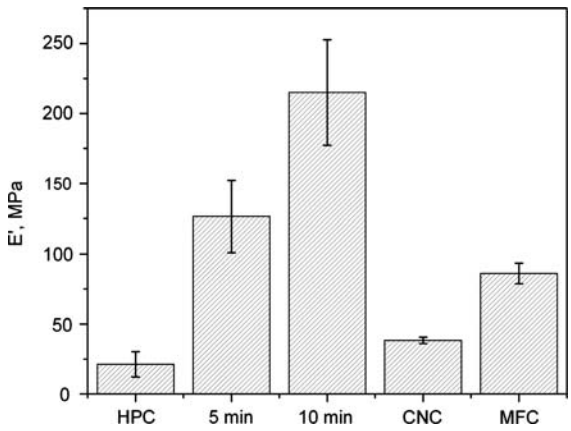

Fig. 9 Storage moduli comparisons at 150 °C for neat HPC and nanocomposites. 5 and 10 min represent sonication times of oxidized pulp suspensions. CNC and MFC represent cellulose nanocrystals and microfibrillated celluloses, respectively

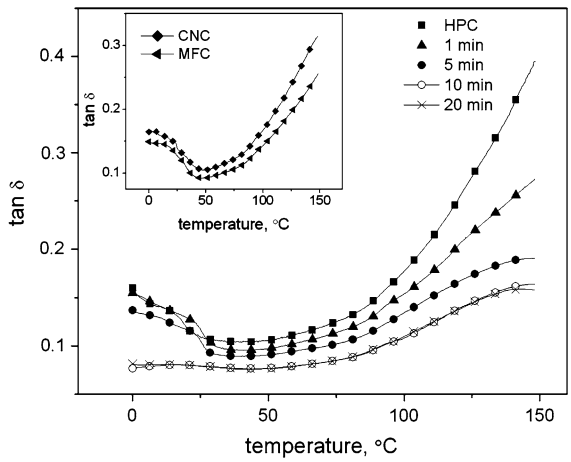

Fig. 10 Tan δ versus temperature of neat HPC and nanocomposites. Sonication times for oxidized pulp suspensions are shown. *Inset* shows corresponding plots for CNCs and MFCs

are of nano-scale dimensions. However, significantly higher E′s are obtained in the TEMPO-oxidized systems sonicated for five or more minutes (Fig. 9). Corresponding tan δ plots (Fig. 10) show portions of two broad thermal transitions (<25 °C and >100 °C). The lower temperature transition is limited to neat HPC and the nanocomposites sonicated for 1 and 5 min. This event corresponds to the glass transition temperature (T_g) of HPC which has been reported as ranging from 10 to 20 °C depending on the characterization method used (Rials and Glasser 1988). Similar T_gs are observed for CNCs and MFCs nanocomposites (inset in Fig. 10). This transition is, however, clearly absent from the nanocomposites sonicated for 10 and 20 min. T_g suppression at high sonication times (i.e. higher nanofibril volume fraction) suggests that HPC interactions with TEMPO-oxidized cellulose nanofibrils may be influenced by the nanofibril volume fraction. The superior performance of TEMPO-oxidized cellulose nanocomposites may be strongly dependent on the unique combination of oxidized cellulose nanofibril characteristics. These include (1) the presence of diverse surface functional groups (OH, CHO, and COO^-) resulting from TEMPO-mediated oxidation, (2) the exceptionally high surface area to volume ratio expected from nanofibril individualization, and (3) the high aspect (length/diameter) ratios evident from TEM imaging (see Fig. 4 and (Saito et al. 2007)). All of these conditions can significantly restrict HPC chain mobility at T_g leading to the observed effects on E′ and tan δ. Future work on TEMPO-oxidized cellulose nanocomposites will look into the role of surface chemical properties on nanocomposite properties.

Time-dependent strain response under static stress conditions is the primary outcome of creep compliance experiments. Tensile creep compliance *D(t)* is the ratio of the time-dependent tensile strain $\varepsilon(t)$ to the applied tensile stress $\sigma_{E,0}$. Ten minute-*D(t)* results of neat and reinforced HPCs at sub-T_g (0 °C) and above T_g (100 °C) regions are shown in Fig. 11. The inset shows a typical set of creep curves collected at 100 °C. Low *D(t)* values with no uniform time-dependence are recorded in the sub-T_g region where HPC chains are essentially frozen. However, at 100 °C, *D(t)* of neat HPC and the nanocomposites increase by approximately two and one order(s) of magnitude, respectively. The nanofibril volume fraction effect is evident from the linear ($R^2 = 0.985$) decrease in *D(t)* as a function of sonication time. Again, compared to CNC and MFC counterparts, the oxidized cellulose nanocomposites exhibit lower *D(t)* at high temperatures (Fig. 12). These observations are consistent with the DMA results discussed previously.

Freeze-fractured cross-sections of HPC and nanocomposite (5 and 20 min sonication) films are displayed in Fig. 13. Nanofibrils were not visible on the fracture surfaces even at very high magnifications. The limits of the SEM resolution were probably reached taking into consideration the combination of

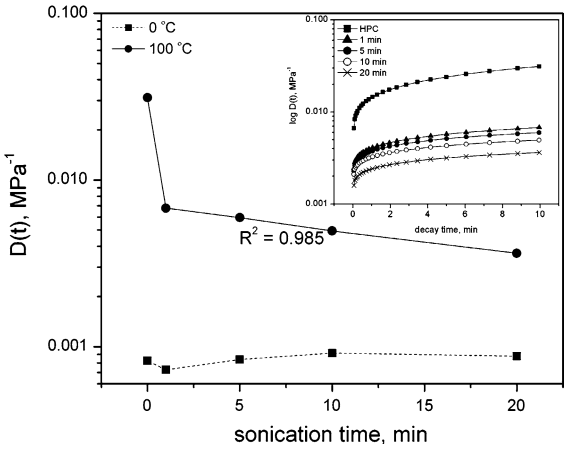

Fig. 11 Tensile creep compliance dependence on sonication time at sub-T_g (0 °C) and above T_g (100 °C) conditions. *Data* represents 10 min creep under 0.6 MPa static stress. 0 min on sonication time axis corresponds to neat HPC. *Inset* shows typical creep curves at 100 °C

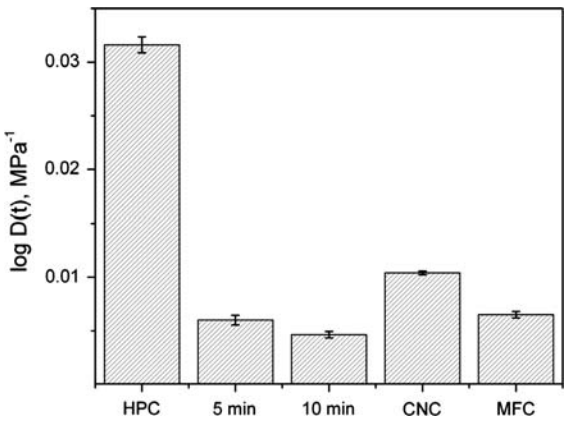

Fig. 12 Comparison of creep compliance at 100 °C of HPC and nanocomposite films. 5 and 10 min represent the sonication times of oxidized pulp suspensions. CNC and MFC represent cellulose nanocrystals and microfibrillated celluloses, respectively

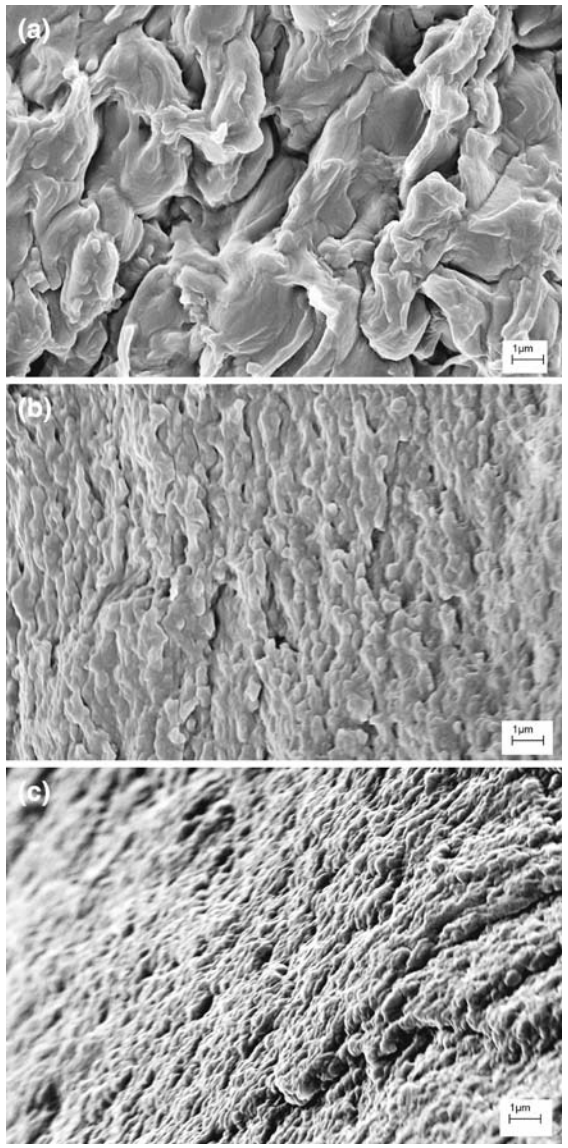

Fig. 13 SEM fracture surfaces of **a** HPC and (**b** and **c**) nanocomposite films. **b** and **c** were fabricated from suspensions sonicated for 5 and (**c**) 20 min, respectively

exceptionally small nanofibril dimensions (3–4 nm) and the thin barrier created by sputter coating. An interesting observation however, is the differences in grain sizes of the surface roughness. Surface roughness grain sizes are significantly reduced on the nanocomposite fracture surfaces compared to neat HPC. Except for the nanocomposites loaded with fibrillated oxidized celluloses sonicated for 1 min (image not shown) where roughness grain sizes were only slightly reduced, all remaining nanocomposite fracture surfaces showed grain sizes similar to those in Fig. 13b and c. Observations similar to this were reported for fracture-toughened intercalated clay-epoxy nanocomposites (Zerda and Lesser 2001). Crack propagation followed a torturous path arising from the very short interparticle distances between clay nanoparticles. It is reported that such toughening mechanisms are not normally observed with fully exfoliated clay (Zilg et al. 1999). However, with intercalated clay, the lateral micron-sized lengths of

the clay nanoplatelets are believed to offer crack bridging mechanisms which are responsible for the tortuous crack propagation behavior. In the present nanocomposites, the surface roughness is observed to be uniform across the sample surface. This may imply, in addition to the interfibrillar distance factor, strong nanofibril-matrix interfaces and uniform nanofibril dispersion. These propositions however, require verification with actual fracture toughness measurements.

Conclusions

Cellulosic nanofibrils from the mechanical disintegration of TEMPO-oxidized celluloses were recently discovered. High intensity sonication was used in this study to control fibrillation of TEMPO-oxidized wood pulp by varying sonication time. Nanocomposite films based on HPC matrix and fibrillated oxidized celluloses were synthesized, characterized, and compared with those from conventional CNCs and MFCs. The conclusions reached are as follows:

1. Based on our selected treatment conditions, 10 min is found sufficient to convert the bulk (*ca*. 90 wt%) of the pulp fibers into nanofibrils.
2. Storage modulus and creep compliance performances of oxidized cellulose nanocomposites exhibit a direct dependence on nanofibril weight fractions, particularly at elevated temperatures.
3. Tan δ data indicate volume fraction-dependent interactions between oxidized cellulose nanofibrils and HPC matrix.
4. Comparison of high temperature E′ performances suggest stronger fibril-matrix interfaces in the oxidized nanofibrils- than conventional (CNCs and MFCs)-filled nanocomposites.
5. Roughness grain sizes of oxidized cellulose-HPC nanocomposite fracture surfaces suggest strong fibril-matrix interface, good fibril dispersion, and probability of crack bridging mechanisms operating at the nanofibril length scales.

Acknowledgments This project was supported by the USDA CSREES Special Grant No. 2006-06204 and the Sustainable Engineered Materials Institute, College of Natural Resources, Virginia Tech, Blacksburg, VA.

References

Beck-Candanedo S, Roman M, Gray DG (2005) Effect of reaction conditions on the properties and behavior of wood cellulose nanocrystal suspensions. Biomacromolecules 6:1048–1054. doi:10.1021/bm049300p

Bragd PL, van Bekkum H, Besemer AC (2004) TEMPO-mediated oxidation of polysaccharides: survey of methods and applications. Top Catal 27:49–66. doi:10.1023/B:TOCA.0000013540.69309.46

Chazeau L, Cavaille JY, Canova G, Dendievel R, Boutherin B (1999) Viscoelastic properties of plasticized PVC reinforced with cellulose whiskers. J Appl Polym Sci 71:1797–1808. doi :10.1002/(SICI)1097-4628(19990314)71:11<1797::AID-APP9>3.0.CO;2-E

Dalmas F, Cavaille JY, Gauthier C, Chazeau L, Dendievel R (2007) Viscoelastic behavior and electrical properties of flexible nanofiber filled polymer nanocomposites. Influence of processing conditions. Compos Sci Technol 67:829–839. doi:10.1016/j.compscitech.2006.01.030

Edgar CD, Gray DG (2003) Smooth model cellulose I surfaces from nanocrystal suspensions. Cellulose 10:299–306. doi:10.1023/A:1027333928715

El-Sakhawy M (2000) Characterization of modified oxycellulose. J Therm Anal Calorim 63:549–558. doi:10.1023/A:1010150122848

Favier V, Chanzy H, Cavaille JY (1995) Polymer nanocomposites reinforced by cellulose whiskers. Macromolecules 28:6365–6367. doi:10.1021/ma00122a053

Gindl W, Keckes J (2005) All-cellulose nanocomposite. Polymer (Guildf) 46:10221–10225. doi:10.1016/j.polymer.2005.08.040

Grunert M, Winter WT (2002) Nanocomposites of cellulose acetate butyrate reinforced with cellulose nanocrystals. J Polym Environ 10:27–30. doi:10.1023/A:1021065905986

Helbert W, Cavaille JY, Dufresne A (1996) Thermoplastic nanocomposites filled with wheat straw cellulose whiskers. 1. Processing and mechanical behavior. Polym Compos 17:604–611. doi:10.1002/pc.10650

Herrick FW, Casebier RL, Hamilton JK, Sandberg KR (1983) Microfibrillated cellulose: morphology and accessibility. J Appl Polym Sci Appl Polym Symp 37:797–813

Katz S, Beatson RP, Scallan AM (1984) The determination of strong and weak acidic groups in sulfite pulps. Sven Papperstidn 87:R48–R53

Kumar V, Yang TR (2002) HNO3/H3PO4-NANO(2) mediated oxidation of cellulose—preparation and characterization of bioabsorbable oxidized celluloses in high yields and with different levels of oxidation. Carbohydr Polym 48:403–412. doi:10.1016/S0144-8617(01)00290-9

Lasseuguette E, Roux D, Nishiyama Y (2008) Rheological properties of microfibrillar suspension of TEMPO-oxidized pulp. Cellulose 15:425–433. doi:10.1007/s10570-007-9184-2

Ljungberg N, Bonini C, Bortolussi F, Boisson C, Heux L, Cavaille JY (2005) New nanocomposite materials reinforced with cellulose whiskers in atactic polypropylene: effect of surface and dispersion characteristics. Biomacromolecules 6:2732–2739. doi:10.1021/bm050222v

Matsumura H, Sugiyama J, Glasser WG (2000) Cellulosic nanocomposites. I. Thermally deformable cellulose hexanoates from heterogeneous reaction. J Appl Polym Sci 78:2242–2253. doi :10.1002/1097-4628(20001220)78:13< 2242::AID-APP20>3.0.CO;2-5

Nakagaito AN, Yano H (2005) Novel high-strength biocomposites based on microfibrillated cellulose having nano-order-unit web-like network structure. Appl Phys Mater Sci Process 80:155–159

Petersson L, Oksman K (2006) Preparation and properties of biopolymer-based nanocomposite films using microcrystalline cellulose. Cellul Nanocompos Process Charact Prop 938:132–150

Petersson L, Kvien I, Oksman K (2007) Structure and thermal properties of poly(lactic acid)/cellulose whiskers nanocomposite materials. Compos Sci Technol 67:2535–2544. doi:10.1016/j.compscitech.2006.12.012

Rials TG, Glasser WG (1988) Thermal and dynamic mechanical-properties of hydroxypropyl cellulose films. J Appl Polym Sci 36:749–758. doi:10.1002/app.1988.070360402

Saito T, Isogai A (2004) TEMPO-mediated oxidation of native cellulose. The effect of oxidation conditions on chemical and crystal structures of the water-insoluble fractions. Biomacromolecules 5:1983–1989. doi:10.1021/bm0497769

Saito T, Nishiyama Y, Putaux JL, Vignon M, Isogai A (2006) Homogeneous suspensions of individualized microfibrils from TEMPO-catalyzed oxidation of native cellulose. Biomacromolecules 7:1687–1691. doi:10.1021/bm060154s

Saito T, Kimura S, Nishiyama Y, Isogai A (2007) Cellulose nanofibers prepared by TEMPO-mediated oxidation of native cellulose. Biomacromolecules 8:2485–2491. doi: 10.1021/bm0703970

Samir MASA, Alloin F, Sanchez JY, El Kissi N, Dufresne A (2004) Preparation of cellulose whiskers reinforced nanocomposites from an organic medium suspension. Macromolecules 37:1386–1393. doi:10.1021/ma030532a

Svagan AJ, Samir MASA, Berglund LA (2007) Biomimetic polysaccharide nanocomposites of high cellulose content and high toughness. Biomacromolecules 8:2556–2563. doi:10.1021/bm0703160

Turbak AF, Snyder FW, Sandberg KR (1983) Microfibrillated cellulose, a new cellulose product: properties, uses, and commercial potential. J Appl Polym Sci Appl Polym Symp 37:815

Varma AJ, Chavan VB (1995) A study of crystallinity changes in oxidized celluloses. Polym Degrad Stab 49:245–250. doi:10.1016/0141-3910(95)87006-7

Wang N, Ding EY, Cheng RS (2007) Thermal degradation behaviors of spherical cellulose nanocrystals with sulfate groups. Polymer (Guildf) 48:3486–3493. doi:10.1016/j.polymer.2007.03.062

Wibowo AC, Misra M, Park HM, Drzal LT, Schalek R, Mohanty AK (2006) Biodegradable nanocomposites from cellulose acetate: mechanical, morphological, and thermal properties. Compos Part A Appl Sci Manuf 37:1428–1433

Wise LE, Murphy M, D'Addieco AA (1946) Chlorite holocellulose, its fractionation and bearing on summative wood analysis and on studies on the hemicelluloses. Pap Trade J 122:11–19

Zerda AS, Lesser AJ (2001) Intercalated clay nanocomposites: morphology, mechanics, and fracture behavior. J Polym Sci Part B Polym Phys 39:1137–1146. doi:10.1002/polb.1090

Zilg C, Mulhaupt R, Finter J (1999) Morphology and toughness/stiffness balance of nanocomposites based upon anhydride-cured epoxy resins and layered silicates. Macromol Chem Phys 200:661–670. doi :10.1002/(SICI)1521-3935(19990301)200:3<661::AID-MACP661>3.0.CO;2-4

Zimmermann T, Pohler E, Geiger T (2004) Cellulose fibrils for polymer reinforcement. Adv Eng Mater 6:754–761. doi: 10.1002/adem.200400097